

MAXI J1820+070: A rapidly spinning black hole with mild disk truncation in the soft state and a warm corona

Th. V. Papavasileiou^{1,2,*}, T. S. Kosmas¹, O. Kosmas³, and I. Sinatkas²

¹ Department of Physics, University of Ioannina, GR-45110 Ioannina, Greece
e-mail: hkosmas@uoi.gr

² Department of Informatics, University of Western Macedonia, GR-52100 Kastoria, Greece
e-mail: th.papavasileiou@uowm.gr, isinatkas@uowm.gr

³ Trumeter Ltd, Pilot Mill, Alfred St, Bury, BL9 9JR Bury, U.K.
e-mail: odykosm@gmail.com

Received <date> / Accepted <date>

ABSTRACT

Context. MAXI J1820+070 is a black hole X-ray binary discovered in 2018 during a major outburst that triggered extensive multi-wavelength observations. Subsequent studies have focused on its physical properties, particularly the black hole spin. In this context, continuum fitting of the source spectra below 25 keV favors low-spin values, whereas spin estimates based on the relativistic precession model and reflection spectroscopy suggest a rapidly rotating black hole.

Aims. Our study seeks to address the debate over the spin of MAXI J1820+070 through broadband (3–79 keV) spectral modeling of NuSTAR observations obtained during the soft state. We further compare our results with previous spin estimates and examine the source variability across the soft state. Finally, we investigate the origin of the soft X-ray excess, which we argue does not originate from the plunge region as previously suggested.

Methods. We adopt a relativistic thin accretion disk model and examine both the phenomenological and physical aspects of the Comptonized tail at higher energies. In addition, we incorporate an appropriate model component for the excess emission below 10 keV, thereby improving the statistical robustness of our fits. To further investigate the origin of this excess, we calculate spin-dependent radial disk temperature profiles across all epochs.

Results. Our results indicate that the black hole in MAXI J1820+070 is rapidly spinning, with spin $a > 0.75$, potentially powering the relativistic jets. Our analysis reveals a significant decline in the inner disk temperature midway through the soft state, accompanied by a modest increase in the inferred inner disk radius up to $\sim 3.5 R_g$. This behavior is consistent with slight disk truncation, possibly associated with a reduction in gas ionization and nonthermal processes. Furthermore, the soft excess emission below 10 keV is well described by a blackbody component at 0.5 keV, approximately 38% cooler than the inner disk. This suggests that the emission may originate from a warm corona layer located beyond $\sim 10 R_g$, analogous to warm Comptonization models proposed to explain the soft X-ray excess in active galactic nuclei.

Key words. MAXI J1820+070 - soft state - NuSTAR observations - black hole spin - accretion disk truncation - blackbody excess - warm corona

1. Introduction

MAXI J1820+070 is a black hole X-ray binary (BHXB) initially discovered in March 2018 as the optical transient ASASSN-18e (Tucker et al. 2018). It was subsequently identified as the optical counterpart of an X-ray transient detected by the MAXI all-sky X-ray monitor aboard the ISS (Kawamuro et al. 2018; Denisenko 2018). The source was later confirmed as a BHXB (Uttley et al. 2018; Baglio et al. 2018b) and associated with a highly variable relativistic jet via optical and infrared variability analysis (Bright et al. 2018; Baglio et al. 2018a; Bright et al. 2020).

The major outburst in 2018, leading to the source’s discovery, remains the primary event providing a wealth of observational data over a timespan of several months. During this period, the source maintained its brightness while undergoing a full spectral state transition (Shidatsu et al. 2018; Shidatsu et al. 2019; Russell et al. 2019). The outburst was so bright, momentarily making MAXI J1820+070 the second brightest X-

ray source in the sky. Several smaller flaring episodes followed in 2019 and 2020, leading to weaker activity reported in the following years (Baglio et al. 2019; Bahramian et al. 2019; Ulowetz et al. 2019; Williams et al. 2019; Hamsch et al. 2019; Adachi et al. 2020; Sasaki et al. 2020; Homan et al. 2023; Baglio et al. 2023).

MAXI J1820+070 is located at a distance of $d = 2.96 \pm 0.33$ kpc and has an inclination of $i = 63 \pm 3^\circ$, based on radio parallax measurements (Atri et al. 2020). Adopting those values, optical spectroscopic analyses yield the black hole and the stellar companion masses as $8.48^{+0.79}_{-0.72} M_\odot$ and $0.61^{+0.13}_{-0.12} M_\odot$, respectively (Torres et al. 2020).

The spin of the black hole in MAXI J1820+070 remains a subject of debate among researchers. Reflection spectroscopy of NICER data obtained during the hard state favors low to moderate spin values (Buisson et al. 2019), a result also supported by Atri et al. (2020). Spectral analysis of NICER and Insight-HXMT data in the 1–25 keV band similarly suggests a low-spin black hole with $a < 0.3$. Specifically, Zhao et al. (2021), fitting Insight-HXMT observations in the 2–25 keV range, derived a

* Corresponding author: th.papavasileiou@uowm.gr

spin of $a = 0.14 \pm 0.09$, while continuum-fitting of a similar dataset by Guan et al. (2021) yielded $a = 0.2_{-0.3}^{+0.2}$. More recent NICER analyses in the 1-10 keV band indicate $a = 0.38 \pm 0.12$, whereas joint fitting with Insight-HXMT data in the 1-25 keV range suggests a slightly lower value of $a = 0.2 \pm 0.1$ (Sai et al. 2024).

Nevertheless, the continuum-fitting results appear to be contradicted by other spin-estimation methods (Rarras et al. 2024). Timing analysis of the NICER data using the relativistic precession model yields a significantly higher black hole spin of $a = 0.799_{-0.015}^{+0.016}$ (Bhargava et al. 2021). Furthermore, multi-epoch NuSTAR analyses employing relativistic reflection spectroscopy indicate that MAXI J1820+070 hosts a near-maximally rotating black hole with $a = 0.988_{-0.028}^{+0.006}$ and a disk inclination of $i = 64_{-4}^{+3}$, consistent with previous estimates (Draghis et al. 2023).

A key difference among these studies lies in the instrument-based datasets and the specific energy ranges covered. Continuum-fitting spin estimates use NICER and Insight-HXMT observations below 25 keV, neglecting most of the Comptonized emission at higher energies. The latter determines how the disk dynamically interacts with the corona, providing a broader view of the source's physical properties (Papavasileiou et al. 2021; Papavasileiou et al. 2023a; Papavasileiou et al. 2023b; Kosmas et al. 2023).

Furthermore, these results are derived on the basis of a relativistic thin accretion disk, whose emission is partially scattered in a power-law tail above 10 keV (Steiner et al. 2009). However, this model does not account for the significant excess emission reported between 6-10 keV (Fabian et al. 2020), which can lead to increased parameter uncertainties and inflated residuals, necessitating the inclusion of systematic errors during spectral fitting. Fabian et al. (2020) modeled the soft X-ray as a blackbody spectrum with $kT = 1$ keV, which is hotter than the inner disk assuming a low spin of $a = 0.2$. Therefore, the emission was speculated to originate near the edge of the plunge region due to magnetic stresses at the innermost stable circular orbit (ISCO).

In this work, we aim to shed light on the spin controversy of MAXI J1820+070 by fitting the entire 3-79 keV NuSTAR bandpass during the 2018 outburst. We perform statistically robust analysis by properly modeling the excess emission below 10 keV and examining the source evolution throughout the soft state, including the potential origin of the blackbody emission. To that end, we calculate the radial temperature profile of the accretion disk and its evolution throughout the soft state, based on the spin-dependent model introduced in our previous work (Papavasileiou et al. 2025).

In the following section (Sec. 2), we describe the data reduction and spectral extraction process. Sec. 3 presents our best-fit results and spectral analysis, while the subsequent sections provide a detailed discussion of the implications of our findings. Finally, we summarise our conclusions in Sec. 7.

2. Data reduction of NuSTAR observations

For our analysis, we selected the NuSTAR observations obtained in July and August 2018, when MAXI J1820+070 was going through the soft state. The observation IDs and their respective exposure times are listed in Table 1. This table also presents the epoch abbreviations adopted throughout this work.

We reduced the data obtained from the HEASARC archive using the most recent `caldb` calibration files and the `nustardas` pipeline tool via the `nupipeline` command. During processing, we applied strict filtering to exclude intervals when the spacecraft passed through the South Atlantic

Table 1: Observational data from NuSTAR during the soft state of MAXI J1820+070. The elapsed time was averaged over both FPMA and FPMB modules.

OBSID	Abbreviation	Duration	Count rate
90401309023	nu23	38.07 ks	461 s ⁻¹
90401309025	nu25	42.86 ks	321 s ⁻¹
90401309027	nu27	83.32 ks	237 s ⁻¹
90401309029	nu29	26.50 ks	158 s ⁻¹
90401309031	nu31	58.66 ks	131 s ⁻¹

Anomaly (SAA), enabling the `saamode` option and activating the `tentacle` flag calculation. Additionally, we applied the standard strict screening criteria, including the expression `(STATUS==b0000xxx00xxx000)&&(SHIELD==0)`, to ensure high data quality. The recommended `SHIELD==0` filter was included to remove cosmic-ray-contaminated events.

After generating the clean event files for both NuSTAR modules (FPMA and FPMB), we used the `nuproducts` command to extract the source and background spectra. The source spectra were obtained from a circular region centered on the source coordinates with a radius of 50 arcsec, while the background spectra were extracted from an annular region with inner and outer radii of 123 and 197 arcsec, respectively. Nonetheless, the background contribution was negligible compared to the source brightness which dominated the spectra across the entire bandpass.

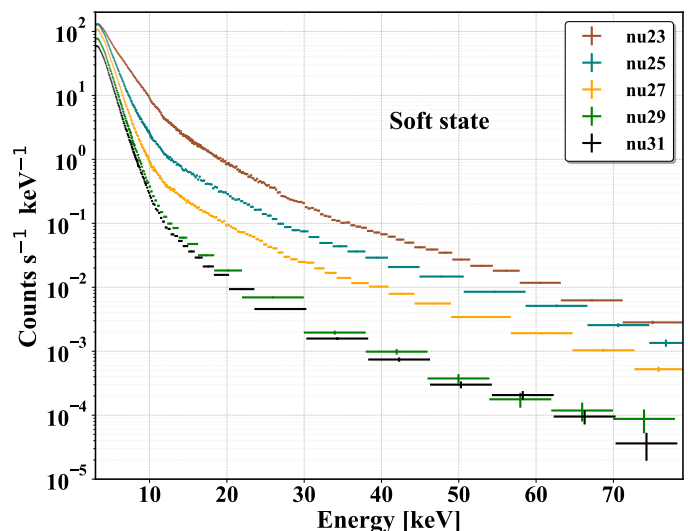


Fig. 1: The merged spectra recorded by the two NuSTAR modules from MAXI J1820+070 in the soft state during the 2018 outburst.

The merged FPMA and FPMB spectra for all epochs are presented in Fig. 1. To ensure the validity of χ^2 statistics, the data were grouped to a minimum of 25 counts per energy bin for spectral fitting. For visualization purposes, the spectra were further rebinned by combining up to 200 channels to achieve at least 30 counts per plotted bin. Notably, epochs nu29 and nu31 exhibit

Table 2: Fixed parameters employed for MAXI J1820+070.

Parameter	MAXI J1820+070	Units
M_{BH}	8.48 (1)	M_{\odot}
d	2.96 (2)	kpc
θ	63 (2)	$^{\circ}$

References. (1) Torres et al. (2020); (2) Atri et al. (2020).

many spectral similarities since the observations occurred only a few days apart.

3. Best-fit results and spectral analysis

We consider the entire 3–79 keV NuSTAR energy range in our fits. All soft-state spectra are fitted separately using two different `xspec` models: `kerrbb+bbbody+cutoffpl` (hereafter Model A) and `kerrbb+bbbody+nthComp` (Model B). Model A is designed to achieve improved statistical convergence, while Model B provides a more physically motivated spectral interpretation. For each epoch, we jointly fit the spectra from the two NuSTAR modules, introducing a cross-calibration constant that is allowed to vary between FPMA and FPMB.

During the fitting procedure, in order to obtain well-constrained spin estimates, we fixed the black hole mass, source distance, and inclination to the most recent values reported for MAXI J1820+070 (see Table 2). The remaining `kerrbb` parameters were kept at their default values. Furthermore, we assume isotropic disk emission and account for self-irradiation of the extended disk (Li et al. 2005). Fig. 2 presents the unfolded spectra for both best-fit models, along with the data-to-model ratios for each epoch.

For the nu23 epoch, a considerable deviation between the data and the model was observed, primarily due to the high count rate and well-documented instrumental calibration uncertainties (Madsen et al. 2021). To mitigate this effect and ensure statistical consistency with the remaining epochs, we imposed a 1.2% systematic error during the fitting procedure.

Overall, the fits are statistically consistent with the data, with reduced χ^2 (i.e., χ^2_{ν}) values ranging between 0.93 and 1.14 for both Model A and Model B. The degrees of freedom for epochs nu23, nu25, nu27, nu29, and nu31 are 2132, 1532, 1586, 677, and 847, respectively. Slightly elevated χ^2_{ν} values in some epochs are primarily driven by minor deviations in the flux above 50 keV. Our best-fit results, along with the parameter uncertainties, are presented in Table 3. For both models, all parameters are well constrained by the data, except for the high-energy cutoff (or equivalently, the electron temperature in the Comptonization component), which becomes increasingly poorly constrained as the spectrum softens.

The disk emission is scattered in the corona, producing a power-law spectrum with an exponential cutoff beyond 40 keV and a spectral index spanning $\Gamma = 1.4$ –2.3. The seed photons, which are thermally Comptonized, originate from a single-temperature disk component with $kT_{bb} = 0.1$ keV. Nonetheless, we verify that even a multi-color disk-appropriate seed emission barely affects the best-fit parameters of Table 3. The temperature of the corona electrons extends approximately from 20 to 30 keV, which is consistent with previous theoretical and observational studies (Burke et al. 2016; Kajava et al. 2016; Jana 2022).

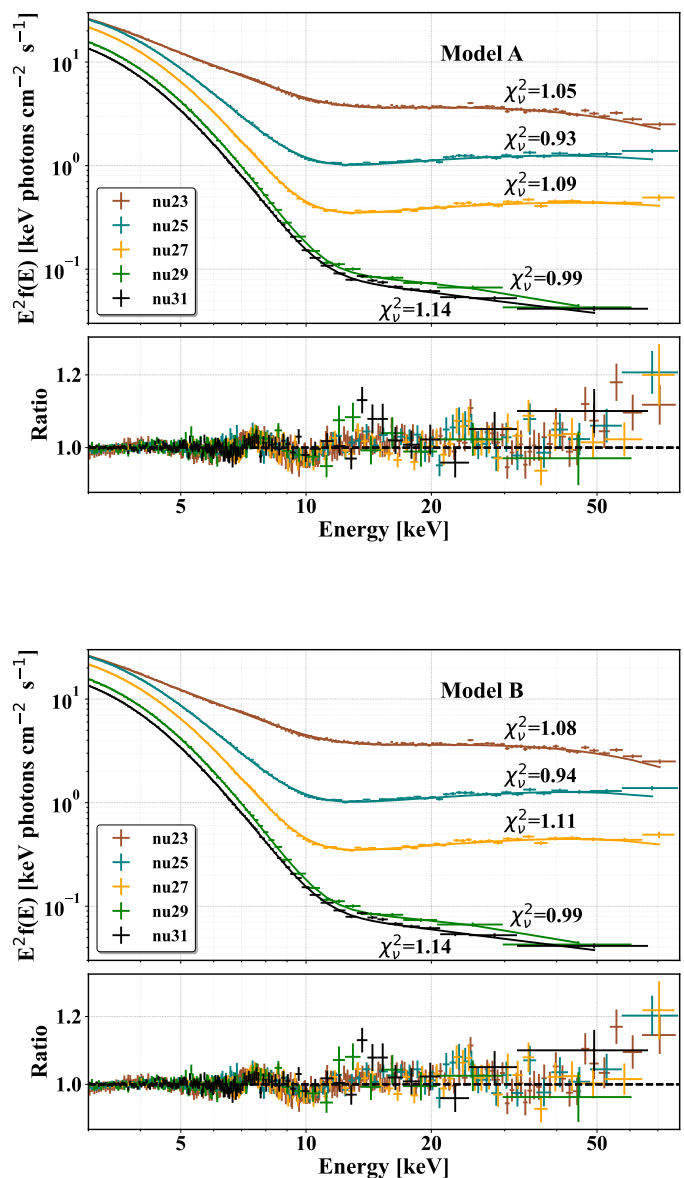


Fig. 2: Spectra from epochs nu23-nu31 unfolded to the best-fit models along with the respective residuals and data-to-model ratios. Top panel: `kerrbb+bbbody+cutoffpl` (Model A), bottom panel: `kerrbb+bbbody+nthComp` (Model B).

Fig. 3 shows the contribution of each spectral component in Models A and B to the nu27 spectral fits. The soft X-ray flux is reproduced by the combined thermal disk emission and the blackbody spectrum at $kT = 0.5$ keV, the latter primarily contributing to the lowest energy bins below the hard X-ray band. The spectral hardening is dominated by nonthermal emission arising from multiple Compton scattering events between the soft disk photons and the hot electron population in the corona above the disk surface.

3.1. Source evolution across the soft state

Fig. 4 illustrates the source evolution throughout the soft state, as inferred from the variance of Model B parameters. The substantial increase in soft thermal flux, associated with the disk extending to the ISCO, enhances Compton cooling and leads to

Table 3: Best-fit results for MAXI J1820+070 throughout the soft state.

OBSID		23	25	27	29	31
Model A: <code>kerrbb+bbbody+cutoffpl</code>						
kerrbb	a	0.999 ± 0.001	$0.905^{+0.016}_{-0.019}$	$0.771^{+0.008}_{-0.049}$	$0.894^{+0.025}_{-0.042}$	$0.958^{+0.011}_{-0.019}$
	Mdd	$0.132^{+0.009}_{-0.005}$	$0.319^{+0.039}_{-0.036}$	$0.514^{+0.094}_{-0.019}$	$0.216^{+0.062}_{-0.035}$	$0.111^{+0.025}_{-0.015}$
blackbody	kT (keV)	$0.476^{+0.004}_{-0.002}$	$0.522^{+0.005}_{-0.002}$	$0.514^{+0.002}_{-0.001}$	$0.508^{+0.003}_{-0.006}$	$0.505^{+0.002}_{-0.004}$
	norm	0.554 ± 0.015	0.498 ± 0.013	$0.351^{+0.006}_{-0.026}$	$0.329^{+0.013}_{-0.021}$	$0.327^{+0.003}_{-0.010}$
cutoffpl	Γ	$1.548^{+0.035}_{-0.044}$	$1.465^{+0.055}_{-0.068}$	1.497 ± 0.045	$1.932^{+0.337}_{-0.250}$	$2.352^{+0.169}_{-0.197}$
	E_{cut} (keV)	$47.87^{+1.02}_{-1.97}$	$75.40^{+16.78}_{-12.65}$	$86.75^{+17.91}_{-13.36}$	$38.13^{+50.53}_{-12.53}$	$128.59 \pm 94.71^*$
	norm	$1.423^{+0.093}_{-0.131}$	$0.295^{+0.035}_{-0.040}$	0.108 ± 0.010	$0.099^{+0.101}_{-0.044}$	$0.201^{+0.078}_{-0.066}$
Model B: <code>kerrbb+bbbody+nthComp</code>						
kerrbb	a	$0.997^{+0.001}_{-0.002}$	$0.876^{+0.028}_{-0.019}$	$0.713^{+0.021}_{-0.010}$	$0.881^{+0.031}_{-0.035}$	$0.956^{+0.012}_{-0.009}$
	Mdd	$0.143^{+0.014}_{-0.007}$	$0.378^{+0.039}_{-0.063}$	$0.628^{+0.029}_{-0.052}$	$0.234^{+0.051}_{-0.044}$	$0.114^{+0.014}_{-0.016}$
blackbody	kT (keV)	0.467 ± 0.007	$0.518^{+0.007}_{-0.004}$	$0.510^{+0.005}_{-0.004}$	$0.506^{+0.005}_{-0.003}$	$0.505^{+0.002}_{-0.003}$
	norm	$0.545^{+0.018}_{-0.016}$	$0.475^{+0.023}_{-0.013}$	$0.319^{+0.014}_{-0.008}$	$0.322^{+0.016}_{-0.017}$	$0.325^{+0.007}_{-0.005}$
nthComp	Γ	1.892 ± 0.012	1.741 ± 0.018	1.736 ± 0.016	$2.215^{+0.149}_{-0.059}$	$2.395^{+0.056}_{-0.111}$
	kT_e (keV)	$20.92^{+1.66}_{-1.24}$	$26.98^{+6.97}_{-3.86}$	$28.41^{+6.99}_{-4.22}$	$18.60^{+40.23}_{-6.19}$	$143.83 \pm 274.20^*$
	norm	$2.642^{+0.096}_{-0.102}$	0.481 ± 0.029	0.164 ± 0.009	$0.159^{+0.072}_{-0.046}$	$0.212^{+0.030}_{-0.047}$

* Parameter unconstrained by the data.

a pronounced decrease in the coronal electron temperature. This results in spectral softening beyond nu27, following the spectral index increase to $\Gamma = 2.2$ – 2.4 . Notably, the high-energy cutoff in Model A evolves consistently with the electron temperature derived from the nthComp component in Model B.

The blackbody emission excess remains fairly steady at $kT \approx 0.5$ keV across all epochs, with a maximum variation of approximately 10% between nu23 and nu25. This suggests that the blackbody-emitting region is physically distinct from the accretion disk and the highly variable corona. However, we will be able to delve deeper into the origin of this emission once we investigate how the temperature profile of the disk evolves throughout the soft state.

4. Spin implications and comparison with previous estimates

Our spectral analysis indicates a high dimensionless black hole spin of $a \approx 0.9$, which exhibits variations throughout the soft state. Specifically, the spin decreases by up to $\sim 38\%$, reaching a minimum of $a \approx 0.7$. This result contrasts with previous continuum-fitting measurements below 25 keV using NICER and Insight-HXMT observations (Zhao et al. 2021; Sai et al. 2024) and timing analysis of QPO frequencies (Fiori et al. 2025). However, it is broadly consistent with mea-

surements obtained through alternative spin-determination techniques (Bhargava et al. 2021; Draghis et al. 2023).

Continuum-fitting analyses of the soft state in MAXI J1820+070 using Insight-HXMT and NICER data indicate considerably lower spins between $a = 0.1$ – 0.3 (Zhao et al. 2021; Guan et al. 2021; Sai et al. 2024). In the first case, the spectra were extracted from the 2–10 keV band of the Low Energy (LE) HXMT instrument and the 10–25 keV band of the Medium Energy (ME) telescope. NICER data cover the 1–10 keV energy band.

Most of the power-law tail lies beyond the energy range used in those studies, limiting the ability to assess the connection between the soft disk emission and subsequent up-scattering at higher energies. This connection is fundamental for determining the spectral properties and, consequently, the physical characteristics of the X-ray binary, including the black hole spin. By comparison, the two almost identical focal plane detector modules of NuSTAR offer simultaneous observational capacity across the entire 3–79 keV bandpass, enhancing the statistical robustness of the analysis.

In most of the studies supporting low spin values, the soft X-ray spectra were fitted using variations of the `tbabs*simpl*kerrbb` model, commonly employed for soft-state spectral analysis. The model produces a relativistic multi-color blackbody spectrum from the accretion disk, account-

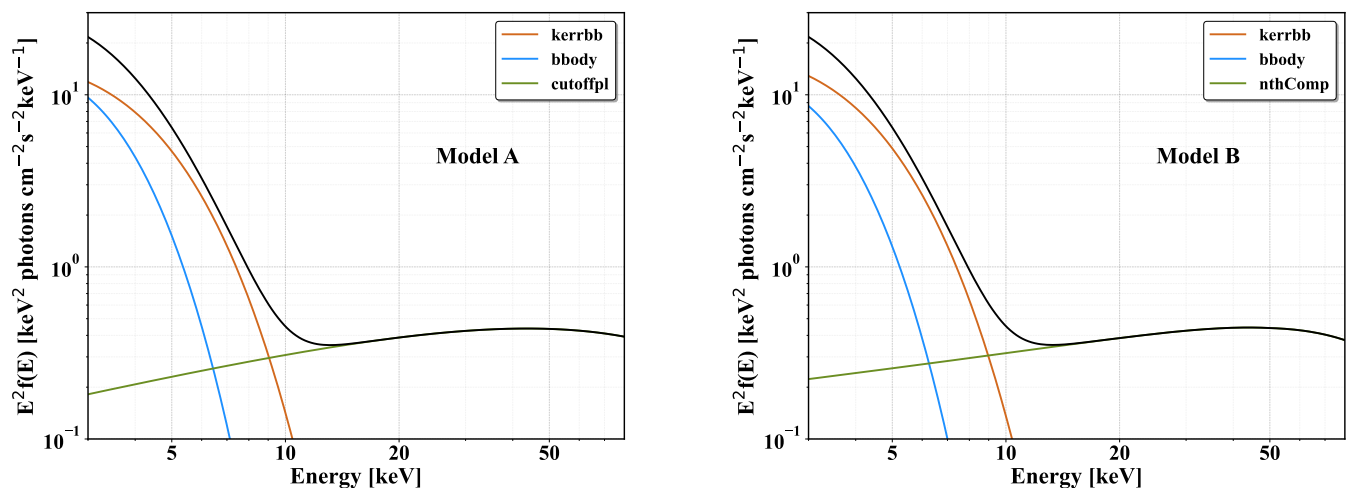


Fig. 3: Contribution of each model component for both Model A (left panel) and Model B (right panel) in the nu27 spectrum. The parameter values employed are the best-fit results of Table 3.

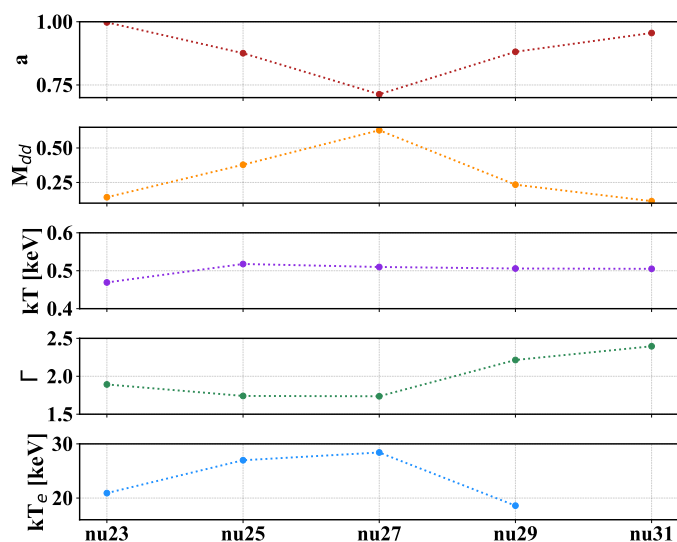


Fig. 4: Source evolution during the soft state based on the variation of the Model B best-fit parameters across all epochs.

ing for galactic absorption. A fraction of the disk emission is Compton-scattered into a high-energy power-law tail (Steiner et al. 2009). Nevertheless, the spectral fits often exhibited residual deviations and substantial spin uncertainties or required systematic errors between 1-2% across all epochs over the entire energy bandwidth.

On the other hand, the `kerrbb+body+cutoffpl` model yields high-quality fits over the broader 3–79 keV bandpass, requiring systematic errors only for the nu23 epoch. Nonetheless, it is disputable whether the extended energy range is statistically more favourable. This does not appear to be the case, as our fits show further improvement below 50 keV (see bottom panels of Fig. 2).

Moreover, to facilitate a fair comparison using NuSTAR data, we fitted our best epoch, nu29, with the `tbabs*simpl*kerrbb` model. We initially fitted the entire 3–79 keV spectrum using `tbabs*(simpl*kerrbb+cutoffpl)`, while keeping the spectral index tied between the `simpl` and

`cutoffpl` components. The resulting fit is statistically reasonable, with $\chi^2/\text{d.o.f} = 743/677 = 1.1$, and the best-fit parameters closely match those of Zhao et al. (2021), suggesting a spin of $a = 0.26$. However, the power-law cutoff occurred at only 1.8 keV, indicating that the model fails to provide an accurate physical interpretation of the observations.

We then restricted the energy band to 3–25 keV, matching the NICER and Insight-HXMT coverage, while omitting the `cutoffpl` component. The resulting fit was significantly worse, with $\chi^2/\text{d.o.f} = 1230/646 = 1.9$. By comparison, fitting the same data with `kerrbb+body+cutoffpl` across all epochs yielded χ^2_ν values between 0.90 and 1.15.

Our results, indicating a high spin of $a > 0.75$, agrees with the QPO frequency evolution derived from NICER power density spectra during the hard state. Application of the relativistic precession model (RPM) gives a spin of $a = 0.799^{+0.016}_{-0.015}$ (Bhargava et al. 2021). Relativistic reflection spectroscopy of multi-epoch NuSTAR data across both primary spectral states indicates a highly rotating black hole with $a = 0.988^{+0.006}_{-0.028}$ and a disk inclination of $\theta = 64^{+3}_{-4}$ (Draghis et al. 2023). This inclination is also consistent with the jet angle determined from radio parallax measurements (Atri et al. 2020), providing further support for the high-spin estimate.

5. Indications of mild disk truncation

The spin evolution during the soft state, as shown in Fig. 4, does not appear to be driven by statistical bias. The inferred spin is initially very high, consistent with a near-maximally rotating black hole. Approximately halfway through the soft state, the spin decreases, before increasing again a few days later during epoch nu29. However, since the black hole spin is not expected to vary over the month-long timescale covered by the NuSTAR observations, we instead investigate whether the apparent spin variability reflects changes in other physical properties of the system. In the `kerrbb` model, the spin parameter is effectively determined by the ISCO radius. Therefore, variations in the estimated spin correspond to changes in the inner disk boundary and its proximity to the event horizon.

Fig. 5 shows the evolution of the inner disk radius across all epochs, as inferred from the best-fit parameters of Model B (see Table 3). The near-maximal prograde spin measured in epoch

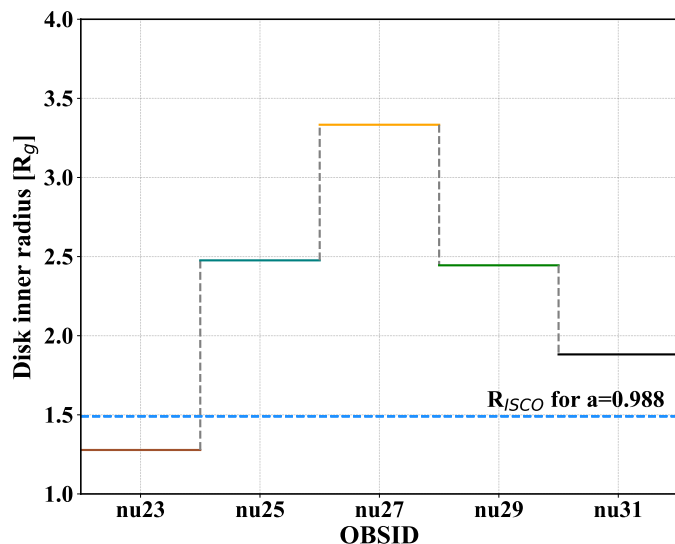


Fig. 5: The evolution of the inner disk radius according to the spin estimations of Model B over epochs nu23–nu31. For comparison, the ISCO radius corresponding to $a = 0.988$ from [Draghis et al. \(2023\)](#) is also plotted.

nu23 corresponds to an accretion disk extending close to the gravitational radius. Subsequently, the disk radius increases to $2.5R_g$ and then to $3.3R_g$ before moving inward again toward the black hole. For comparison, we also plot the ISCO radius corresponding to $a = 0.988$ ([Draghis et al. 2023](#)). Adopting this spin, the offset between the horizontal reference line and the inferred inner disk radii in Fig. 5 suggests that the accretion disk might not consistently extend to the ISCO, but instead undergoes slight truncation during the soft state.

Nevertheless, the aforementioned potential structural changes in the disk could instead reflect intrinsic modifications in the physical state of the accreting gas. Previous studies have supported that spectral evolution between state transitions could be attributed to color correction instead of the commonly speculated disk truncation ([Salvesen et al. 2013](#); [Zdziarski et al. 2022](#)). In the innermost regions, the accretion flow can reach temperatures between 10^5 – 10^7 K, leading to strong ionization and a regime in which electron scattering dominates over thermalization interactions. This results in spectral hardening, which is accounted for, in the multi-color disk framework, through the color correction factor, $f_{col} = T_{col}/T_{eff} = 1.2$ – 1.9 (denoted as hd in the `kerrbb` model) ([Li et al. 2005](#)). In our analysis, this parameter was fixed at its default value of $f_{col} = 1.7$ ([Shimura & Takahara 1995](#)).

To further investigate this possibility, we refit all NuSTAR epochs with Models A and B by fixing the spin to $a = 0.988$ and allowing f_{col} to vary. The best-fit parameters are reported in Table 4 and plotted in Fig. 6. The remaining model parameters stay consistent with those listed in Table 3. The softer spectra observed during epochs nu25–nu29 can be interpreted as arising from a cooler, weakly-ionized accretion flow near the black hole that does not allow for very intense electron scattering. Consequently, the degree of spectral hardening is reduced, and the corresponding factor ranges between $f_{col} = 1.2$ – 1.4 . Throughout the soft state, the parameter lies between $f_{col} = 1.2$ – 1.8 , consistent with [Davis & El-Abd \(2019\)](#), who report values between 1.4 – 2.0 when $0.01 \leq L/L_{Edd} \leq 1$.

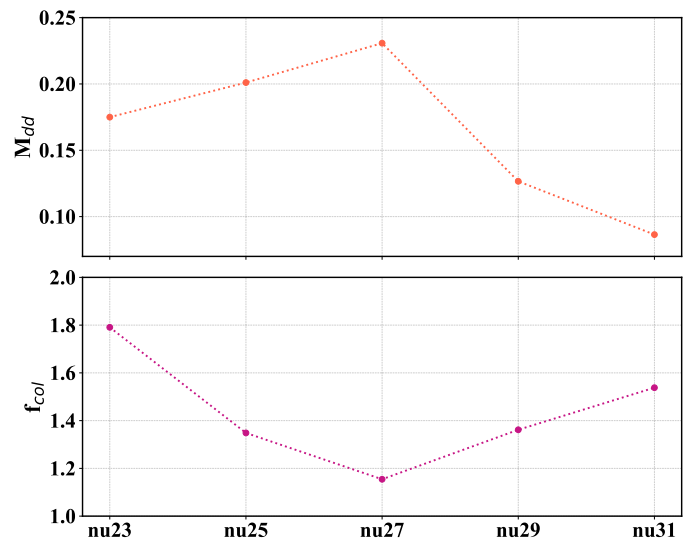


Fig. 6: Evolution of the mass accretion rate and color correction factor across the soft state when the black hole spin is fixed at $a = 0.988$.

5.1. Disk truncation or gas thermalization?

It is evident that an abrupt drop in the temperature of the inner disk regions occurs midway through the soft state (nu27), which cannot be explained solely by variations in the accretion rate. This behavior may be attributed to mild truncation of the disk boundary, a reduction in electron scattering or other non-thermal interactions in the accreting gas (as encapsulated by f_{col}), or a combination of both effects. Further examination of both prospects motivates us to investigate how the disk temperature profile evolves across all epochs. However, the `kerrbb` model does not provide direct access to this quantity, since T_{in} is not an explicit model parameter, unlike in the `diskbb` model.

In [Papavasileiou et al. \(2025\)](#), we adopted the pseudo-Newtonian gravitational potential introduced by [Artemova et al. \(1996\)](#) to derive a spin-dependent temperature–radius relation for accretion disks around rotating black holes. The resulting temperature profile is written as ([Papavasileiou et al. 2025](#))

$$T_A(r) = T_0 \left(\frac{(3 - \beta)(r - r_h) + \beta r}{3r^{3-\beta}(r - r_h)^{\beta+1}} \right)^{1/4} (1 - \mathcal{A})^{1/4}, \quad (1)$$

where r is the radius normalized by the gravitational radius, $r_h = 1 + \sqrt{1 - a^2}$ is the event horizon depending on the spin, and $\beta = r_{in}/r_h - 1$ ([Artemova et al. 1996](#)). The quantity within the brackets is given by

$$\mathcal{A} = \left(\frac{r_{in}}{r} \right)^{(\beta+1)/2} \left(\frac{r - r_h}{r_{in} - r_h} \right)^{\beta/2}. \quad (2)$$

The disk temperature scales as

$$T_0 = \left(\frac{3GM_{bh}\dot{M}}{8\pi\sigma R_g^3} \right)^{1/4}. \quad (3)$$

By adopting a fixed spin (and hence a fixed inner radius) of $a = 0.988$, we plot in Fig. 7 the disk temperature profiles from Eq. 1 corresponding to each NuSTAR observational epoch. Initially, the disk is significantly hotter, with temperatures reaching 1 keV

Table 4: Best-fits for $a = 0.988$ and a varying color correction factor f_{col} , denoted as `hd` in `kerrbb`.

OBSID		23	25	27	29	31
Model A: <code>kerrbb+bbbody+cutoffpl</code>						
<code>kerrbb</code>	<code>Mdd</code>	0.177 ± 0.004	0.189 ± 0.012	0.221 ± 0.011	0.122 ± 0.013	0.087 ± 0.006
	<code>f_{col}</code>	1.832 ± 0.029	1.397 ± 0.043	1.178 ± 0.025	1.384 ± 0.061	1.537 ± 0.050
Model B: <code>kerrbb+bbbody+nthComp</code>						
<code>kerrbb</code>	<code>Mdd</code>	0.175 ± 0.004	0.201 ± 0.012	0.231 ± 0.011	0.127 ± 0.012	0.086 ± 0.006
	<code>f_{col}</code>	1.791 ± 0.028	1.348 ± 0.038	1.154 ± 0.022	1.362 ± 0.057	1.538 ± 0.045

($\approx 10^7$ K), but it cools down abruptly, leading to a simultaneous heating of the corona (see Table 3). This trend continues up to epoch `nu27`, where the disk experiences slight reheating before the soft state gradually fades out.

The temperature profiles for each epoch in Fig. 7 can be represented by a single profile shifted outward, suggesting a rapid structural change in the accretion disk. While variations in f_{col} can account for the observed cooling, the mechanism triggering such an abrupt partial rethermalization of the gas remains unclear. A modest disk truncation to a maximum radius of $\sim 3.5R_g$ could induce a substantial drop in gas temperature and a corresponding increase in density, weakening non-blackbody effects within the accretion flow and causing a decrease in f_{col} , although smaller than indicated in Table 4.

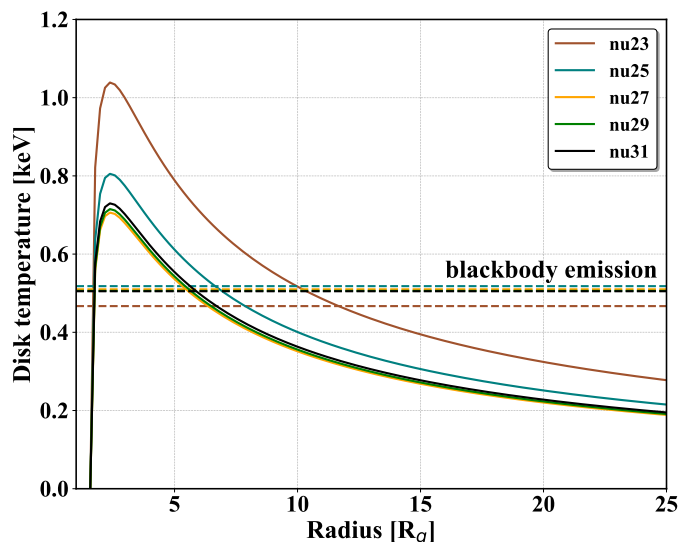


Fig. 7: Disk temperature evolution across the soft state, considering the black hole spin is $a = 0.988$ and the inner radius is constant. The same temperature evolution can be reproduced by a gradual outward shift of the disk boundary. In addition, the blackbody spectrum temperature is plotted, indicating a cooler emission source than the inner disk regions.

Similar spectral variability, indicating low-temperature disk emission despite high luminosities, is observed in the very high states of black hole binaries. In these cases, it was speculated that an optically thick, extended corona partially obscured the inner disk. However, explaining the observed spectra required a substantial increase in the inner disk radius. An alternative explanation involves a disk–corona coupling model, which reproduces the observed features more accurately (Done & Kubota 2006). Even so, a slight increase in the inner disk radius remains necessary to account for the observations, supporting our claim of minor disk truncation. In this scenario, the corona must be optically thick and extend over a large portion of the innermost, hotter regions of the disk, potentially linking it to the blackbody excess observed below 10 keV.

6. Origin of blackbody excess emission

Fabian et al. (2020), analyzing the 2018 NuSTAR dataset, concluded that the soft excess originated near the edge of the plunge region. Their spectral fitting with the `diskbb+bbbody+cutoffpl` model revealed a blackbody excess with $kT \approx 1$ keV, while the inner disk temperature was only 0.6 keV. During this fitting, an inner disk boundary at $5R_g$ was assumed, corresponding to a spin of $a \approx 0.2$, and an inclination of $i = 34^\circ$, based on the hard-state spectral analysis of Buisson et al. (2019). These assumptions conflict with the inclination of 63° reported by Atri et al. (2020) and with arguments supporting a high-spin black hole.

In our case, the spin was allowed to vary, leading to spectral fits that suggest $a > 0.75$, in agreement with X-ray reflection spectroscopy estimates. Employing our generalized spin-dependent temperature profile (Eq. 1) for accretion disks, we find that the blackbody excess source is not hotter than the inner accretion disk. Instead, it is in thermal equilibrium with the region around $10R_g$ (see Fig. 7), ruling out the plunge region assumption.

A soft X-ray excess near 1 keV has been consistently reported in various active galactic nuclei (AGNs). This emission is commonly modeled as a blackbody, although its purely thermal origin is disputed due to its constant temperature that does not scale with the black hole mass and luminosity. Consequently, the soft excess is often attributed either to ionized reflection from the inner disk surface or to thermal Comptonization by a warm corona above the disk (Petrucci et al. 2018; Ding et al. 2021).

The latter is the most widely accepted explanation, assuming a warm corona with temperatures between $kT = 0.1-1$ keV and optical depths of $\tau = 10-40$. In this scenario, the corona reprocesses the UV/optical emission from the inner disk, producing a quasi-thermal excess in the soft X-ray band (Petrucci et al. 2018; Ding et al. 2021).

The blackbody excess in MAXI J1820+070 spans the 1-10 keV energy range and maintains a nearly constant temperature of 0.5 keV (Fig. 7), independent of luminosity. This behavior suggests that a mechanism similar to that in AGNs may produce the soft excess in XRBs. Even in low-spin systems, the warm corona temperature would not exceed 1 keV. A key difference is that the inner disk in XRBs is considerably hotter, causing Compton cooling rather than thermal Comptonization. Consequently, the seed photons responsible for the blackbody excess must originate from cooler disk regions below 0.5 keV, which, according to Fig. 7, lie at radii beyond $\sim 10R_g$ from the black hole.

Moreover, the corona layer is marginally heated after the initial phase of the state (Fig. 7), plausibly by the significantly hotter accretion gas via advective mechanisms. The small temperature change suggests that the layer must cover an extended portion of the disk surface, consistent with warm Comptonization models in AGNs (Petrucci et al. 2018).

7. Conclusions

The spin of the black hole in MAXI J1820+070 remains a persistent and debated issue. Continuum-fitting of the source's soft-state spectra generally indicates a low spin ($a < 0.3$), whereas alternative methods, including reflection spectral analysis and the relativistic precession model, favor a higher spin ($a > 0.75$). A major distinction between those studies is the adopted instrument-driven datasets and their respective energy band. Continuum-fitting estimations and relativistic precession were based on NICER and Insight-HXMT observations, while reflection spectroscopy was applied on a broad NuSTAR dataset that includes the outburst during 2018.

We aim to resolve this debate by applying the continuum-fitting method to the soft X-ray spectra from the source, obtained by NuSTAR during the summer of 2018. Our best-fit models were statistically robust, with reduced χ^2 values ranging from 0.93 to 1.14 across all epochs, requiring no systematic errors except for a single epoch.

Our results indicate that the black hole in MAXI J1820+070 is rapidly rotating, with a spin of $a > 0.75$, consistent with X-ray reflection spectroscopy and relativistic precession analysis (Bhargava et al. 2021; Draghis et al. 2023). This finding contradicts previous continuum-fitting estimates (Zhao et al. 2021; Guan et al. 2021; Sai et al. 2024). The reason is that, in those studies, the spectra covered the 1-25 keV range, which is a portion of the NuSTAR bandpass (3-79 keV), but most notably, the models employed for the spectral fits were variations of the `tbabs*simpl*kerrbb` configuration that fails to justify the excess emission below 10 keV. In our case, the latter is fitted by a single blackbody spectrum at a consistent temperature of 0.5 keV throughout the soft state.

To verify our results, we refitted our best-performing epoch in the 3-25 keV band, matching the energy range of NICER and Insight-HXMT, using the `tbabs*simpl*kerrbb` model. The best-fit parameters closely matched those reported by Zhao et al. (2021). However the residuals were $\chi^2_\nu = 1.9$, substantially higher compared to our fits in the same energy band.

Our analysis reveals a substantial drop in the inner disk temperature midway through the soft state, which manifests as an

apparent spin variation. This change in emission flux cannot be explained solely by variations in the accretion rate. Assuming a fixed spin of $a = 0.988$ (Draghis et al. 2023), the inferred spin evolution may instead reflect either a modest outward shift of the disk's inner boundary to a maximum radius of $3.5R_g$, or a pronounced decrease in the ionization state and nonthermal interactions within the accreting gas. The latter scenario is consistent with a reduction in the color correction factor to $f_{col} \approx 1.2-1.4$. Even so, the abrupt gas rethermalization could itself be partially triggered by modest disk truncation.

The blackbody excess emission below 10 keV is consistent with the presence of a warm, optically thick corona with a temperature of approximately 0.5 keV located above the disk. This interpretation is analogous to warm Comptonization models invoked to explain the soft X-ray excess in active galactic nuclei. By applying the spin-dependent temperature profile derived in Papavasileiou et al. (2025), we are able to determine that the warm corona layer resides at radii $R > 10R_g$, potentially extending over a substantial fraction of the disk surface.

References

- Adachi, R., Murata, K. L., Oeda, M., et al. 2020, *The Astronomer's Telegram*, 13502, 1
- Artemova, I. V., Bjoernsson, G., & Novikov, I. D. 1996, *ApJ*, 461, 565
- Atri, P., Miller-Jones, J. C. A., Bahramian, A., et al. 2020, *Monthly Notices of the Royal Astronomical Society: Letters*, 493, L81
- Baglio, M. C., Russell, D. M., Alabarta, K., et al. 2023, *The Astronomer's Telegram*, 16192, 1
- Baglio, M. C., Russell, D. M., Casella, P., et al. 2018a, *ApJ*, 867, 114
- Baglio, M. C., Russell, D. M., & Lewis, F. 2018b, *The Astronomer's Telegram*, 11418, 1
- Baglio, M. C., Russell, D. M., Qaisieh, T. A., et al. 2019, *The Astronomer's Telegram*, 12596, 1
- Bahramian, A., Motta, S., Atri, P., & Miller-Jones, J. 2019, *The Astronomer's Telegram*, 12573, 1
- Bhargava, Y., Belloni, T., Bhattacharya, D., Motta, S., & Ponti, G. 2021, *Monthly Notices of the Royal Astronomical Society*, 508, 3104
- Bright, J., Fender, R., & Motta, S. 2018, *The Astronomer's Telegram*, 11420, 1
- Bright, J. S., Fender, R. P., Motta, S. E., et al. 2020, *Nature Astronomy*, 4, 697
- Buisson, D. J. K., Fabian, A. C., Barret, D., et al. 2019, *Monthly Notices of the Royal Astronomical Society*, 490, 1350
- Burke, M. J., Gilfanov, M., & Sunyaev, R. 2016, *Monthly Notices of the Royal Astronomical Society*, 466, 194
- Davis, S. W. & El-Abd, S. 2019, *The Astrophysical Journal*, 874, 23
- Denisenko, D. 2018, *The Astronomer's Telegram*, 11400, 1
- Ding, N., Gu, Qisheng, Tang, Yunyong, et al. 2021, *A&A*, 650, A183
- Done, C. & Kubota, A. 2006, *Monthly Notices of the Royal Astronomical Society*, 371, 1216
- Draghis, P. A., Miller, J. M., Zoghbi, A., et al. 2023, *The Astrophysical Journal*, 946, 19
- Fabian, A. C., Buisson, D. J., Kosec, P., et al. 2020, *Monthly Notices of the Royal Astronomical Society*, 493, 5389
- Fiori, M., Zampieri, L., Burtovoi, A., et al. 2025, *A&A*, 697, A222
- Guan, J., Tao, L., Qu, J. L., et al. 2021, *Monthly Notices of the Royal Astronomical Society*, 504, 2168
- Habsch, J., Ulowetz, J., Vanmunster, T., Cejudo, D., & Patterson, J. 2019, *The Astronomer's Telegram*, 13014, 1
- Homan, J., Baglio, M. C., Saikia, P., et al. 2023, *The Astronomer's Telegram*, 16200, 1
- Jana, A. 2022, *Monthly Notices of the Royal Astronomical Society*, 517, 3588
- Kajava, J. J. E., Veledina, A., Tsygankov, S., & Neustroev, V. 2016, *A&A*, 591, A66
- Kawamuro, T., Negoro, H., Yoneyama, T., et al. 2018, *The Astronomer's Telegram*, 11399, 1
- Kosmas, O., Papavasileiou, T., & Kosmas, T. 2023, *Universe*, 9
- Li, L.-X., Zimmerman, E. R., Narayan, R., & McClintock, J. E. 2005, *The Astrophysical Journal Supplement Series*, 157, 335
- Madsen, K. K., Forster, K., Grefenstette, B. W., Harrison, F. A., & Miyasaka, H. 2021, 2021 Effective Area calibration of the Nuclear Spectroscopic Telescope ARray (NuSTAR)
- Papavasileiou, T., Kosmas, O., & Sinatkas, I. 2021, *Galaxies*, 9
- Papavasileiou, T., Kosmas, O., & Sinatkas, I. 2023b, *Universe*, 9
- Papavasileiou, T. V., Kosmas, O., & Kosmas, T. S. 2025, *A&A*, 693, A75

- Papavasileiou, T. V., Kosmas, O. T., & Sinatkas, I. 2023a, *Astron. Astrophys.*, 673, A162
- Petrucchi, P.-O., Ursini, F., De Rosa, A., et al. 2018, *A&A*, 611, A59
- Rarras, D., Kosmas, O., Papavasileiou, T., & Kosmas, T. 2024, *Particles*, 7, 818
- Russell, D. M., Baglio, M. C., & Lewis, F. 2019, *The Astronomer's Telegram*, 12534, 1
- Sai, N., Wang, W., & Wu, H. 2024, *Journal of High Energy Astrophysics*, 43, 44
- Salvesen, G., Miller, J. M., Reis, R. C., & Begelman, M. C. 2013, *Monthly Notices of the Royal Astronomical Society*, 431, 3510
- Sasaki, R., Negoro, H., Nakahira, S., et al. 2020, *The Astronomer's Telegram*, 13530, 1
- Shidatsu, M., Nakahira, S., Murata, K. L., et al. 2019, *ApJ*, 874, 183
- Shidatsu, M., Nakahira, S., Yamada, S., et al. 2018, *The Astrophysical Journal*, 868, 54
- Shimura, T. & Takahara, F. 1995, *ApJ*, 445, 780
- Steiner, J. F., Narayan, R., McClintock, J. E., & Ebisawa, K. 2009, *Publications of the Astronomical Society of the Pacific*, 121, 1279
- Torres, M. A. P., Casares, J., Jiménez-Ibarra, F., et al. 2020, *The Astrophysical Journal Letters*, 893, L37
- Tucker, M. A., Shappee, B. J., Holoiien, T. W.-S., et al. 2018, *The Astrophysical Journal Letters*, 867, L9
- Ulowetz, J., Myers, G., & Patterson, J. 2019, *The Astronomer's Telegram*, 12567, 1
- Uttley, P., Gendreau, K., Markwardt, C., et al. 2018, *The Astronomer's Telegram*, 11423, 1
- Williams, D., Motta, S., Bright, J., et al. 2019, *The Astronomer's Telegram*, 12577, 1
- Zdziarski, A. A., You, B., & Szanecki, M. 2022, *The Astrophysical Journal Letters*, 939, L2
- Zhao, X., Gou, L., Dong, Y., et al. 2021, *The Astrophysical Journal*, 916, 108